

CERN-TH/95-148  
 hep-ph/9506233

## DETERMINATION OF $\alpha_s$ FROM $F_2^p$ AT HERA

Richard D. Ball\* and Stefano Forte†

*Theory Division, CERN,  
 CH-1211 Genève 23, Switzerland.*

### Abstract

We compute the proton structure function  $F_2^p$  at small  $x$  and large  $Q^2$  at next-to-leading order in  $\alpha_s(Q^2)$ , including summations of all leading and subleading logarithms of  $Q^2$  and  $1/x$  in a way consistent with momentum conservation. We perform a detailed comparison to the 1993 HERA data, and show that they may be used to determine  $\alpha_s(M_Z^2) = 0.120 \pm 0.005(\text{exp}) \pm 0.009(\text{th})$ . The theoretical error is dominated by the renormalization and factorization scheme ambiguities.

Submitted to: *Physics Letters B*

CERN-TH/95-148

hep-ph/9506233

May 1995

---

\* On leave from a Royal Society University Research Fellowship.

† On leave from INFN, Sezione di Torino, Italy.

Experimental knowledge of the proton structure function  $F_2$  at large  $Q^2$  and small  $x$  has dramatically improved since data from HERA have become available [1,2]. Whereas the data are in beautiful agreement [3] with the leading-order prediction of perturbative QCD [4], and in particular display the double scaling behaviour which follows [5] from it, the improvement in experimental accuracy now opens up the possibility of more detailed tests of the theory. Indeed, reliable perturbative calculations in the small  $x$  region turn out to be possible thanks to the fact that perturbation theory can be reorganized to give an evolution equation which provides order by order a convergent sum of all leading logarithms of  $x$  and  $Q^2$  [6]. Here we will show that full next-to leading order (NLO) computations give an excellent description of all the HERA data. Furthermore, this description is largely independent of any detailed nonperturbative (thus uncalculable) information, such as the detailed shape of input parton distributions, but is relatively sensitive to the precise value of the strong coupling  $\alpha_s$ , which may thus be determined using presently available data [7].

The determination of  $\alpha_s$  from the shape of  $F_2^p$  at small  $x$  which we will discuss here is similar to that used in the analysis of large  $x$  structure functions, however it also shares some of the features of measurements based on less inclusive quantities (see ref. [8]). In fact, many of the more inclusive measurements (for example  $e^+e^- \rightarrow$  hadrons) require precise data with very high statistics, since it is necessary to measure the small  $Q^2$ -dependent deviations from an  $\alpha_s$ -independent leading order result. The determinations from scaling violations in structure functions obtained from fixed target deep inelastic scattering are even more difficult, since there the leading behaviour (the parton distribution functions at some initial scale) cannot be reliably computed, but must be fitted. By contrast, measurements based on less inclusive quantities which are essentially proportional to  $\alpha_s$  at leading order (for example jet rates, event shapes and energy correlations) can be made with much lower statistics: the dominant error then comes from hadronization uncertainties. In this respect the determination of  $\alpha_s$  from  $F_2^p$  at small  $x$  discussed here is akin to the jet determination, and, in particular, it can be made with relatively low statistics; however here there are no hadronization effects, and higher twist corrections will turn out to be relatively small.

The possibility of determining  $\alpha_s$  from the presently available HERA data [1,2] for  $F_2^p(x, Q^2)$  follows directly from the empirical fact that the data exhibit double scaling [5]: throughout the HERA kinematic region  $\ln F_2^p$  rises linearly in  $\sigma \equiv \sqrt{\xi\zeta}$ , but is independent of  $\rho \equiv \sqrt{\xi/\zeta}$  (where, as in ref.[5],  $\xi \equiv \ln \frac{x_0}{x}$ ,  $\zeta \equiv \ln \frac{t}{t_0}$ ,  $t \equiv \ln Q^2/\Lambda^2$ ). More precisely,  $R_F F_2$ , where  $R_F$  is proportional to  $\sigma^{1/2} \rho \exp(-2\gamma\sigma + \delta\sigma/\rho)$ , is independent of both  $\sigma$  and

$\rho$ . This may be seen immediately from the scaling plots fig. 1. The two parameters  $\gamma \equiv \sqrt{12/\beta_0}$ ,  $\delta \equiv (11 + \frac{2n_f}{27})/\beta_0$  depend inversely on the rate of running of  $\alpha_s(t) = \frac{4\pi}{\beta_0 t} + O(\frac{1}{t^2})$ ;  $\beta_0 = 11 - \frac{2}{3}n_f$  is the leading coefficient of the  $\beta$ -function. The fact that the HERA data exhibit double scaling is thus direct evidence for the running of  $\alpha_s(t)$  [3]. Furthermore, the growth of  $F_2$  at small  $x$  and large  $Q^2$  is due primarily to the collinear singularity in the triple gluon vertex [4] (at leading order in perturbation theory), and it is thus directly and simply related to the actual value of  $\alpha_s$ . This is seen most clearly by rewriting the predicted [4,5] asymptotic leading order behaviour of  $F_2^p$  as

$$F_2^p \sim \mathcal{N} \xi^{-3/4} \left[ \ln \frac{\alpha_s(t_0)}{\alpha_s(t)} \right]^{1/4} \left( \frac{\alpha_s(t)}{\alpha_s(t_0)} \right)^\delta \exp \left\{ 2\gamma \sqrt{\xi} \sqrt{\ln \frac{\alpha_s(t_0)}{\alpha_s(t)}} \right\} \left( 1 + O(\alpha_s(t)) \right). \quad (1)$$

Since the third term rises more slowly than any power of  $\alpha_s$ , at very large  $t$  (and fixed  $x$ ) the second term dominates and Bjorken scaling is eventually recovered. However at smaller values of  $t$  and small enough values of  $x$  (and in particular in the HERA region [5]) the strong growth in the third term overwhelms the power fall-off in the second, and  $F_2$  rises quickly as  $\alpha_s$  falls. It is this strong dependence of the leading behaviour of  $F_2$  at small  $x$  on the value of  $\alpha_s$  which makes it possible to make a precise determination of  $\alpha_s$  using the existing HERA data [1,2]. Indeed, fitting the functional form (1) to the data, fixing  $Q_0 = 1$  GeV and  $x_0 = 0.1$ , as in [5], gives  $\alpha_s(M_Z) = 0.125 \pm 0.002$  (at one loop), with a  $\chi^2$  of 68/121, which is at least encouraging.

Of course, to actually determine  $\alpha_s$  requires at least a full NLO computation, in order to fix the scale. Indeed, a two loop computation [9] reveals that NLO effects lead to a reduction in rate of growth of  $F_2$  in the HERA region: although the asymptotic slope  $2\gamma$  is approached at very large  $\sigma$ , subasymptotically the slope is somewhat lower. This is essentially due to the fact that the leading singularity in the two-loop splitting function  $P_1^{gg}$  is of opposite sign to that at leading order: in  $\overline{\text{MS}}$  scheme

$$P^{gg}(x, t) = \left[ 2C_A - \frac{(46C_A - 12C_F)T_R n_f}{9} \frac{\alpha_s(t)}{2\pi} \right] \frac{1}{x} + \dots, \quad (2)$$

where  $C_A = 3$ ,  $C_F = \frac{4}{3}$ ,  $T_R = \frac{1}{2}$  for  $N_c = 3$ . The slope of the rise in  $F_2$  is accordingly reduced. Indeed this reduction can now be seen in the data (see table 4 and fig. 1): agreement with the data is significantly improved, essentially because of the progressive fall in the  $\sigma$  plot. This suggests that a consistent (i.e. reasonably scale independent) determination of  $\alpha_s$  is indeed going to be possible.

However, in the small  $x$  region, i.e. when two large scales are present ( $Q^2$  and the centre of mass energy of the partonic scattering process  $s = \frac{1-x}{x}Q^2$ ) a NLO computation may be performed in a variety of inequivalent expansion schemes, which correspond to different ways of organizing the perturbative expansion [6]. The standard two loop computation, where only logs of  $Q^2$  are considered leading, is one such expansion scheme, whereas other schemes are obtained by also including logs of  $1/x$ . Unlike different factorization or renormalization schemes, which are equivalent up to higher order perturbative corrections, different expansion schemes can lead to physically inequivalent predictions because they sum up different classes of logarithms. A comparison with the data may thus allow one to decide in which region each expansion scheme is physically most appropriate.

The fact that the HERA data agree well with the double scaling prediction (1), which treats the two large scales on the same footing (retaining only terms with the same number of powers of  $\log Q^2$ ,  $\log \frac{1}{x}$ , and  $\alpha_s$ ) suggests that the most appropriate expansion scheme in the HERA region is the double leading scheme [6], where one sums all contributions to splitting functions where each power of  $\alpha_s$  is accompanied by either a power of  $\log Q^2$  or  $\log \frac{1}{x}$ , i.e. the two scales are still treated symmetrically. At leading order this means that one should keep all terms with either one power of  $\alpha_s$  or any number of powers of  $\alpha_s \log \frac{1}{x}$ , and at NLO all terms with an extra power of  $\alpha_s$ . The singlet splitting functions are then of the form<sup>1</sup>

$$\begin{aligned} P^{ij}(x, t) &= P_{\text{LO}}^{ij}(x) + \frac{\alpha_s(t)}{2\pi} P_{\text{NLO}}^{ij}(x, t) + \dots, \\ P_{\text{LO}}^{ij}(x) &= P_1^{ij}(x) + P_s^{ij}(x, t) \quad P_{\text{NLO}}^{ij} = P_2^{ij}(x) + P_{ss}^{ij}(x, t), \end{aligned} \tag{3}$$

where  $P_1^{ij}(x)$  and  $P_2^{ij}(x)$  are the usual one and two loop splitting functions, while  $P_s^{ij}(x, t)$

---

<sup>1</sup> In the standard notation in which the evolution of the singlet parton distribution functions  $f^i(x, t)$  is given by  $\frac{d}{dt}f^i = \frac{\alpha_s}{2\pi}P^{ij} \otimes f^j$ : different conventions were used in refs.[5,6].

and  $P_{ss}^{ij}(x, t)$  are (convergent) sums of leading and subleading singularities respectively:

$$\begin{aligned}
P_s^{gg}(x, t) &= 2C_A \frac{1}{x} \sum_{n=3}^{\infty} a_{n+1} \frac{1}{n!} \lambda_s(t)^n \xi^n, \\
P_s^{gq}(x, t) &= \frac{C_F}{C_A} P_s^{gg}(x, t), \quad P_s^{qg}(x, t) = P_s^{qq}(x, t) = 0, \\
P_{ss}^{qg}(x, t) &= \frac{16}{3} \ln 2C_A T_R n_f \frac{1}{x} \sum_{n=1}^{\infty} \tilde{a}_{n+1} \frac{1}{n!} \lambda_s(t)^n \xi^n, \\
P_{ss}^{qq}(x, t) &= \frac{C_F}{C_A} P_{ss}^{qg}(x, t), \\
P_{ss}^{gg}(x, t) &= 16 \ln 2C_A^2 \frac{1}{x} \sum_{n=1}^{\infty} b_{n+1} \frac{1}{n!} \lambda_s(t)^n \xi^n, \\
P_{ss}^{gq}(x, t) &= 16 \ln 2C_A C_F \frac{1}{x} \sum_{n=1}^{\infty} b'_{n+1} \frac{1}{n!} \lambda_s(t)^n \xi^n,
\end{aligned} \tag{4}$$

where  $\lambda_s(t) \equiv 4 \ln 2 \frac{C_A}{\pi} \alpha_s(t)$ ,  $\alpha_s(t)$  is the two-loop running coupling, and  $\xi = \log \frac{x_0}{x}$  for  $x < x_0$ , zero otherwise.

Similar expansions are taken for the singlet coefficient functions

$$C^{ij}(x, t) = \delta^{ij} \delta(1 - x) + \frac{\alpha_s(t)}{2\pi} (C_1^{ij}(x) + C_s^{ij}(x, t)) + \dots, \tag{5}$$

where  $C_1^{ij}(x)$  are the usual two-loop coefficient functions, while

$$\begin{aligned}
C_s^{qg}(x, t) &= \frac{2}{3} T_R n_f \frac{1}{x} \sum_{n=1}^{\infty} c_n \frac{1}{(n-1)!} \lambda_s(t)^n \xi^{n-1}, \\
C_s^{qq}(x, t) &= \frac{C_F}{C_A} C_s^{qg}(x, t), \quad C_{ss}^{gg}(x, t) = -C_{ss}^{qg}(x, t), \quad C_{ss}^{gq}(x, t) = -C_{ss}^{qq}(x, t).
\end{aligned} \tag{6}$$

The nonsinglet splitting functions and nonsinglet coefficient function remain the same as at two loops; there are no singular contributions in the nonsinglet channels, except in singular factorization schemes [10].

The coefficients  $a_n$  in (4) may be deduced [11] from the BFKL kernel by means of appropriate factorization theorems [12]; a similar technique for computing  $\tilde{a}_n$  and  $c_n$  has been developed in [13,14,15]. However, unlike the  $a_n$ , the coefficients  $\tilde{a}_n$  and  $c_n$ , being subleading, depend on which renormalization and factorization schemes are adopted. In ref. [14] calculations are performed in  $\overline{\text{MS}}$ , but results are also given in a corresponding parton scheme (DIS) in which the gluon contribution to  $F_2$  is eliminated altogether, the  $c_n$  are zero and  $C^{ij}(x, t) = \delta^{ij} \delta(1 - x)$ . Furthermore, the process independent singularity in the DIS quark anomalous dimensions, which is what makes the corresponding  $\tilde{a}_n$  so large,

can be eliminated by a suitable redefinition of the normalization of the gluon distribution, thereby greatly reducing the coefficients  $\tilde{a}_n$ ; this normalization (and thus this form of the anomalous dimension) is automatically given by off-shell factorization of collinear singularities ( $Q_0$  factorization) [16]. This factorization prescription thus defines an alternative parton scheme which we call  $Q_0$ DIS. It is also then possible to construct a  $Q_0\overline{\text{MS}}$  scheme, in which the anomalous dimensions (and thus the  $\tilde{a}_n$ ) are the same as those in the  $\overline{\text{MS}}$  scheme, but the process independent singularity in the coefficient functions is eliminated, reducing the  $c_n$ . Finally, it is even possible to construct a parton scheme in which both the  $\tilde{a}_n$  and the  $c_n$  are zero (the singular DIS or SDIS scheme) [17]; all subleading singularities in the quark channel are then factorized into the starting distribution.

Analytic expressions for the first fourteen coefficients  $a_n$  may be found in the second of ref. [12], and for the first five  $\tilde{a}_n$ ,  $c_n$  in [14], while the first fourteen  $\tilde{a}_n$  and twelve  $c_n$  in  $\overline{\text{MS}}$  may be found in table 2 and table 3. Analytic expressions for the  $\tilde{a}_n$  in DIS scheme are readily deduced from tables 2 and 3, and the corresponding expressions in the  $Q_0$ DIS scheme may be computed similarly. Numerical values for the first thirty-two  $a_n$ , and  $\tilde{a}_n$  in DIS are given in [6]; in table 1 we give also the first twenty  $\tilde{a}_n$  and the corresponding  $c_n$  in  $\overline{\text{MS}}$ , the  $c_n$  in  $Q_0\overline{\text{MS}}$ , and the  $\tilde{a}_n$  in  $Q_0$ DIS.<sup>2</sup>

The coefficients  $b_n$  and  $b'_n$  which appear in the expansion of the NLO singular splitting functions  $P_{ss}^{gg}$  and  $P_{ss}^{qq}$  have not yet been explicitly computed in any scheme. However, when working at NLO in the double leading scheme no computation is really necessary, since the requirement of momentum conservation determines these coefficients uniquely. Indeed, in any subtraction scheme in which there is a detailed balance of momentum between quarks and gluons, the splitting functions must satisfy the relations

$$\int_0^1 dx x [P^{qg}(x, t) + P^{gg}(x, t)] = 0, \quad \int_0^1 dx x [P^{qg}(x, t) + P^{gq}(x, t)] = 0, \quad (7)$$

for all  $t$ . This equation cannot be satisfied at leading order, since  $P_s^{qg} = P_s^{gq} = 0$ , but at NLO it determines<sup>3</sup>

$$b_n = b'_n = -a_{n+1} - \frac{T_R n_f}{3C_A} \tilde{a}_n. \quad (8)$$

---

<sup>2</sup> These latter coefficients are obtained [16] in practice by simply suppressing the singular process independent  $R_N$  factors in the expressions in ref. [13-15].

<sup>3</sup> Note that if these coefficients were computed explicitly in a given renormalization and factorization scheme the result would not necessarily agree with eq. (8) and thus would not conserve momentum at NLO in the double leading expansion. However, it is always possible to then perform a change of factorization scheme such that momentum conservation is restored at NLO, and thus eq. (8) is satisfied.

This procedure can be extended to any finite order: for example at NNLO  $P_{ss}^{gg}$ ,  $P_{ss}^{gq}$ ,  $P_{sss}^{gg}$  and  $P_{sss}^{gq}$  would be computed in  $\overline{\text{MS}}$ , and then  $P_{sss}^{gg}$  and  $P_{sss}^{gq}$  would be fixed by momentum conservation. Notice that at NLO this prescription automatically preserves the colour-charge relation

$$P_{ss}^{gq}(x, t) = \frac{C_F}{C_A} P_{ss}^{gg}(x, t); \quad (9)$$

it is then easy to check explicitly that because of the colour-charge relations between  $P^{gq}$  and  $P^{gg}$ ,  $P^{qg}$  and  $P^{gg}$  the supersymmetry relation

$$P^{qg}(x, t) + P^{gq}(x, t) = P^{qg}(x, t) + P^{gg}(x, t), \quad (10)$$

holds when  $C_F = C_A = 2T_R$ .

Whereas the double leading expansion scheme discussed so far is appropriate to the HERA region, it is clearly inadequate at large  $x$ : there, in order to improve the two-loop expressions of splitting functions, it would be necessary to compute the full three loop contributions  $P_3^{ij}$  and  $C_2^{ij}$ , while to include only those higher order contributions which have small  $x$  singularities is meaningless. Below a reference value  $x_0$  the ordinary loop expansion scheme should thus be used instead, so the singular contributions  $P_s^{ij}$ ,  $P_{ss}^{ij}$  and  $C_s^{ij}$  should all vanish there. Imposing that at  $x = x_0$  the splitting functions and coefficient functions should be continuous, while for  $x < x_0$  the logarithmic singularities are built up asymptotically as the evolution length  $x_0/x$  increases, then leads naturally to the expressions (4) and (6).<sup>4</sup> We will assume for simplicity that the parameter  $x_0$  which sets the transition to the small  $x$  region is independent of  $t$ . We then treat it as a free parameter, to be eventually determined empirically. Naively we would expect it to lie in the range  $0.01 \lesssim x_0 \lesssim 0.1$ , at least for all reasonable schemes; here we will thus consider the extreme case  $x_0 = 0.1$ , the opposite extreme being given in effect by the

---

<sup>4</sup> Note that in [5,6] we defined the separation of the evolution region and introduced different expansion schemes in different regions at the level of the evolution equation, by implicitly evolving the parton distribution functions at large  $x$  to give the boundary condition at  $x = x_0$  from which they were then evolved using an expansion scheme appropriate to small  $x$ . Here the separation is done instead at the level of the evolution kernel, thus making the separation into large and small- $x$  regions on the basis of the evolution length (in  $x$ ). The present prescription has the advantage that it may be used in Mellin space, since the evolution remains translationally invariant. The two prescriptions however are identical by construction when  $x > x_0$ , and only differ by subleading corrections in  $\xi$  when  $x < x_0$ .

two loop computation (for which  $x_0 = 0$ ). Notice that this parameter will in general be factorization and renormalization scheme dependent, and should for instance be smaller in  $\overline{\text{MS}}$  (which has large values of  $c_n$  and  $\tilde{a}_n$ ) than in the  $Q_0\overline{\text{MS}}$  scheme.

Since the expansions (4) and (6) are convergent, they may in practice be truncated after only a finite number of terms: when working in Mellin space arbitrarily accurate results may thus be obtained by truncating the corresponding series expansions of the anomalous dimensions [6] (even though these series have only a finite radius of convergence, diverging for small  $N$ ). Defining  $\gamma^{ij}(N, t) \equiv \int_0^1 dx x^N P^{ij}(N; t)$  term by term, we thus have

$$\begin{aligned} \gamma_s^{gg}(N, t) &\simeq 2C_A x_0^{-N} \sum_{n=4}^{n_{\max}} a_n \lambda_s(t)^{n-1} / N^n, \\ \gamma_s^{gq}(N, t) &= \frac{C_F}{C_A} \gamma_s^{gg}(N, t), \quad \gamma_s^{qg}(N, t) = \gamma_s^{qq}(N, t) = 0, \\ \gamma_{ss}^{qg}(N, t) &\simeq \frac{16}{3} \ln 2C_A T_R n_f x_0^{-N} \sum_{n=2}^{n_{\max}} \tilde{a}_n \lambda_s(t)^{n-1} / N^n, \\ \gamma_{ss}^{gg}(N, t) &\simeq -16 \ln 2C_A^2 x_0^{-N} \sum_{n=2}^{n_{\max}} (a_{n+1} + \frac{T_R n_f}{3C_A} \tilde{a}_n) \lambda_s(t)^{n-1} / N^n, \\ \gamma_{ss}^{qq}(N, t) &= \frac{C_F}{C_A} \gamma_{ss}^{qg}(N, t), \quad \gamma_{ss}^{qg}(N, t) = \frac{C_F}{C_A} \gamma_{ss}^{gg}(N, t). \end{aligned} \quad (11)$$

The renormalization group equation may then be integrated explicitly, while the inverse Mellin transform is straightforward because the anomalous dimensions (11) are meromorphic in  $N$ : in particular there are no extra singularities or branch cuts [6].<sup>5</sup> Care must be taken to ensure that all the subleading contributions are consistently linearized in this solution (even across thresholds). It is important to notice that this applies to the full NLO contribution, and not only to its large- $x$  part; the effect of the spurious sub-subleading terms which would otherwise be produced may in practice be quite large.

In order to actually perform the computation of  $F_2^p$  we use a suitable generalization of the general procedure developed for two loops calculations in ref. [9]. We take a set of parton distribution functions  $\Delta = \{f(x, 4\text{GeV}^2) : f = v, q, g, \dots, x > 10^{-2}\}$  fitted to all available data with  $Q^2 \gtrsim 4\text{GeV}^2$ ,  $x \gtrsim 10^{-2}$  which predates the HERA data and is thus unbiased by it: in practice we work with the two MRS distributions D0' and D-' [19]. We then evolve these distributions to some new scale  $Q_0^2$ , and refit the resulting parton distribution functions  $\{f(x, Q_0^2) : f = v, q, g, \dots, x > 10^{-2}\}$  to functions of the same form

---

<sup>5</sup> A quite complicated set of branch cuts are present in the analytic continuation of the complete series from large  $N$  [18].

as the original distributions, but with the small  $x$  behaviour of the singlet sea and the glue distributions now fixed to be  $x^\lambda$  for some  $\lambda$ :

$$\begin{aligned} xq(x, Q_0^2) &= A_q x^{\lambda_q} (1-x)^{\eta_q} (1 + \epsilon_q x^{1/2} + \gamma_q x), \\ xg(x, Q_0^2) &= A_g x^{\lambda_g} (1-x)^{\eta_g} (1 + \epsilon_g x^{1/2} + \gamma_g x). \end{aligned} \quad (12)$$

We thus obtain a new set of distributions  $[\Delta](Q_0, \lambda)$  which when evolved up to larger values of  $Q^2$  will give (almost) precisely the same results for  $x \gtrsim 10^{-2}$  as the original distribution  $\Delta$  (perturbative evolution being ‘causal’ both in  $t$  and  $1/x$ ) but different results for  $x \lesssim 10^{-2}$ . The functions  $[\Delta](Q_0, \lambda)$  can actually be fitted to parton distributions  $\{f(x, Q_0^2)\}$  defined either in the  $\overline{\text{MS}}$  or in a parton scheme; possible differences in the results will then depend on the approximation introduced by the choice of the specific functional form of eq. (12).

Numerical computations can now be performed in Mellin space using a straightforward extension to  $n_{\text{max}}$  loops of the standard two loop solution [20] of the renormalization group equations, with the form eq. (11) of the small- $x$  contributions to the anomalous dimensions. We have checked explicitly that the evolved parton distributions converge as  $n_{\text{max}}$  is increased: very accurate results in the HERA region may be obtained using only the coefficients given in table 4, for all values of  $x_0$ . Due to the universality of double scaling we expect the results to be insensitive to the detailed form of the starting distributions; the only significant constraint imposed by the large- $x$  data is the overall normalization of the small- $x$  tail. The data can thus be fitted by simply adjusting the parameters  $Q_0$ ,  $\lambda_q$  and  $\lambda_g$ , taken within suitable ranges.

Let us first consider the two loop case (or, equivalently, double leading schemes with  $x_0 = 0$ ) in the  $\overline{\text{MS}}$  scheme. We begin by assuming for simplicity  $\lambda_q = \lambda_g = \lambda$ . Still, the set of free parameters  $(Q_0, \lambda)$  is somewhat redundant. To understand how this works, we present in fig. 2a a  $\chi^2$  contour plot in the  $\lambda - Q_0$  plane. All the 46 ZEUS [1] and 76 H1 [2] bins which pass the cut  $\sigma, \rho > 1$  are included in the computation of the  $\chi^2$ ; the cuts are imposed in order to only include small  $x$  data. The normalization of each experiment is also fitted, in accordance with the experimental uncertainty<sup>6</sup>. Clearly, a good fit can be obtained for a variety of values of the starting scale  $Q_0$ ; the valley floor then defines  $\lambda$  as a function of  $Q_0$  (or alternatively, of course, the other way around). As noted in [9],

---

<sup>6</sup> A useful discussion of the appropriate treatment of normalization uncertainties may be found in [21].

reasonable results at two loops may be obtained when  $\lambda(Q_0)$  vanishes at  $Q_0 \sim 1$  GeV; starting at a higher scale the best fit value increases, being around  $\lambda = -0.2$  if  $Q_0 \simeq 2$  GeV, consistent with the most recent MRS global fit [22]. What really matters however is not so much the precise value of  $\lambda$ , but that the data prefer soft starting distributions, which necessarily give rise to double scaling in the HERA region: as explained in [5] if the starting distribution is too hard, say  $\lambda(1 \text{ GeV}^2) \lesssim -0.2$  or  $\lambda(4 \text{ GeV}^2) \lesssim -0.4$ , double scaling is spoiled and a satisfactory fit to the data is no longer obtained. Similarly the fit gets worse if one attempts to describe the data using a power at a much higher scale.

In table 4 we show thus the best fit value of the parameter  $\lambda$  obtained in the  $\overline{\text{MS}}$  scheme at various values of  $Q_0$ . Whereas the double scaling prediction of ref. [5] with  $Q_0 = 1$  GeV already provides a good overall description of the data, the fit improves in a statistically significant way when the full two loop calculation is performed, especially if, consistent with the  $\chi^2$  plot of fig. 2a, we choose a somewhat larger starting scale. The improvement in the fit is also apparent in the corresponding two loop curves in the scaling plot fig. 1. Evolution in DIS scheme at two loops gives almost identical results.

We now proceed to NLO calculations in the double leading expansion scheme with  $x_0 = 0.1$ , and in the various factorization and renormalization schemes discussed above. The result found in the SDIS scheme (which differs from the two loop computation DIS only for the inclusion of gluon leading singularities  $\gamma_s^{gg}$  (11)) are effectively indistinguishable from those obtained at two loops<sup>7</sup> (at least in the range of present-day data); we will thus not discuss this case further here. If the  $Q_0\overline{\text{MS}}$  scheme is used instead the best-fit value of the parameter  $\lambda$  changes appreciably; however the impact on the quality of the fit does not appear to be statistically significant. If we use instead the double leading  $\overline{\text{MS}}$  scheme, the agreement with the data of the present fit is significantly worse. This, however, turns out to be a byproduct of the specific way we are parametrizing the boundary conditions.

In order to understand this, we present in table 5 the results of fits analogous to those discussed so far, but where now we fit the small- $x$  exponents of the quark and gluon distributions (12),  $\lambda_q$  and  $\lambda_g$  as two independent parameters. Furthermore, we fit the functional form of eq. (12) to parton distributions in either  $\overline{\text{MS}}$  or parton schemes; in order to disentangle effects due to the fitting from the true scheme dependence we then evolve both sets of distributions in both  $\overline{\text{MS}}$  and parton schemes. It then turns out that

---

<sup>7</sup> This is partly because the first few  $a_n$  vanish, but also because the others are very small, so that their effect is concentrated in a very narrow wedge close to the boundary [6].

in some schemes (and in particular in the double leading  $\overline{\text{MS}}$  scheme) a good fit is only possible if the values of  $\lambda_q$  and  $\lambda_g$  are substantially different. In particular, at two loops with the fitted distribution in  $\overline{\text{MS}}$   $\lambda_q \simeq \lambda_g$ , but if the distribution is fitted in DIS  $\lambda_q$  is significantly lower than  $\lambda_g$ . In the double leading expansion the situation is reversed:  $\lambda_q \simeq \lambda_g$  in DIS, but  $\lambda_g$  is very significantly lower than  $\lambda_q$  in  $\overline{\text{MS}}$ .<sup>8</sup> However, if the double leading calculation is performed with  $Q_0$  factorization, then  $\lambda_q \simeq \lambda_g$  in either case. Notice that this is genuinely an effect of the fitting, in that all of the above remains true regardless of whether the evolution is performed in  $\overline{\text{MS}}$  or in a parton scheme.

We conclude that in general the results of the double leading calculations do not differ significantly from those obtained at two loops. This means that, while the leading singularities  $P_s^{gg}$  have essentially no effect at all, most of the effect of the subleading singularities  $P_{ss}^{qg}$  on  $F_2$  in the HERA region may be absorbed into the boundary condition, generally reducing  $\lambda$  and increasing  $Q_0$ . The HERA data on  $F_2^p$  thus do not as yet actually allow us to fix the value of  $x_0$ . However, the boundary conditions themselves do change significantly as we go from two loops to the double leading scheme; furthermore, in the double leading scheme they display very strong scheme dependence. This is of course the essence of factorization: since the boundary condition at  $Q_0^2$  is essentially nonperturbative and scheme dependent, it must always be fitted in a comparison with the data, and furthermore it may change substantially when different factorization and renormalization schemes are adopted. This however has also the practical consequence that we may only reasonably take  $\lambda_q = \lambda_g \equiv \lambda$  in the fitted distribution if we fit  $\overline{\text{MS}}$  distributions at two loops, and DIS distributions in the double leading scheme, unless we use  $Q_0$  factorization, in which case we may use either. In order to avoid artificial complications related to the fitting procedure we shall thus henceforth perform two loop computations (fitting and, for definiteness, evolution) in  $\overline{\text{MS}}$  and double leading computations in parton schemes; this will allow us to take  $\lambda_q = \lambda_g = \lambda$  throughout.

We can now explore in more detail the  $Q_0$  dependence of  $\lambda$  in the double leading DIS scheme, as summarized in the  $\chi^2$  contour plot fig. 2b. The best fit  $\lambda$  at a given scale is significantly reduced in comparison with the two loop case fig. 2a because  $F_2$  grows

---

<sup>8</sup> It is interesting to notice that the best fit  $\lambda_g$  is then rather large; nevertheless scaling is not spoilt. This agrees with the results of ref. [6], where we show that although at two loops only  $\lambda_g \gtrsim -0.3$  leads to scaling, in the double leading scheme any  $\lambda_g \gtrsim -\lambda_s(Q_0)$  is sufficient.

more quickly near the boundary as  $Q^2$  is increased.<sup>9</sup> The scale  $Q_0$  at which a given (soft) boundary condition should be set is thus correspondingly increased [6]: the results obtained then differ very little from the two loop fits, except at large  $\rho$  i.e. very close to the boundary itself, as displayed by the pertinent curves in fig. 1. Furthermore, because of the more significant role played by perturbative evolution, the double leading fit is more sensitive to the choice of  $Q_0$ . However, the fit is less sensitive to the precise value of  $\lambda$ . This somewhat surprising result was anticipated in ref. [6] where it was shown that actually double scaling is obtained from a wider set of initial conditions if a full double leading computation is performed than would be the case at two loops.

It is now relatively straightforward to determine  $\alpha_s$  from the HERA data on  $F_2$ : we simply include an extra parameter  $\Lambda_{\text{QCD}}$  (or equivalently  $\alpha_s(M_Z)$ ) in the fit. The results of such two parameter fits, for the various NLO calculations described above are displayed in table 6. The experimental uncertainty in the resulting value of  $\alpha_s(M_Z)$  turns out to be remarkably small, of the order of a few per cent. The value of the starting scale  $Q_0$  is seen to have little effect on the value of  $\alpha_s(M_Z)$ , though  $\lambda(Q_0^2)$  varies rather strongly when  $Q_0$  is below 2 GeV (see fig. 2).

The dependence on  $Q_0$  and  $\lambda$  is explored in detail in the  $\chi^2$  plots in the two planes perpendicular to that of fig. 2: the  $\alpha$  -  $\lambda$  plane fig. 3, and the  $Q_0$ - $\alpha$  plane fig. 4. The well-defined minimum in  $\lambda$  and  $\alpha_s(M_Z)$  is apparent from fig. 3a; large values of  $\alpha_s$  are excluded much more strongly when the subleading singularities are included fig. 3b. The flatness of the valley floor in fig. 4 reflects that in fig. 2, but again the acceptable range of  $Q_0$  is significantly reduced when the subleading singularities are included in the calculation. In general all double leading calculations seem to be significantly more sensitive to the values of the parameters; even though they cannot yet be favoured on statistical grounds they could thus potentially lead to a firmer determination of  $\alpha_s$ . For the time being, however, we determine the central value of  $\alpha_s$  from the fits with the best  $\chi^2$ , namely, the two loop calculations. An average of these (see table 6) gives a central value  $\alpha_s(M_Z) = 0.120$ . The uncertainty related to the possibility of choosing various expansion schemes is then asymmetric, since double leading schemes tend to lead to a reduction of  $\alpha_s$ ; from table 6 we estimate it to be  $+0.002 - 0.006$ .

---

<sup>9</sup> Very low values of the starting scale  $Q_0$  (as favoured by [23], for example) would seem to be excluded in these schemes, because their effect when  $\alpha_s(Q_0^2)$  is large is too great to admit a satisfactory fit to the data even with valence-like input (large positive  $\lambda$ ).

We now examine all other sources of error in turn. The sensitivity to the form of the starting distributions is explored by considering different choices of large  $x$  distributions (for example the two ‘extremal’ MRS distributions  $D0'$  and  $D-'$  [19]), and also more importantly by varying the way in which the small- $x$  tail is fitted to these distributions at  $Q_0$ . In particular, choosing  $\lambda_s \neq \lambda_g$  has little effect on  $\alpha_s$  (see table 7). Two alternative fitting procedures have also been tried: one in which a small- $x$  tail of the form  $x^\lambda$  is added by hand to the singlet distributions  $xq(x, Q_0^2)$ ,  $xg(x, Q_0^2)$  before the refitting (which is then performed over the extended range  $x > 10^{-4}$ ), the normalization of the tail being fixed by continuity, and a similar one in which the tail has instead the form  $x^\lambda(1 + \epsilon\sqrt{x})$ , the parameters  $\epsilon_q$  and  $\epsilon_g$  being chosen such that the derivatives of the two distributions were continuous at the matching point (see again table 7). Estimating the error from all these sources rather conservatively at  $\pm 0.003$ , and combining it in quadrature with an error of  $\pm 0.003$  from the two parameter fit, and  $\pm 0.002$  from the choice of  $Q_0$  (see table 6), we feel confident in quoting an overall experimental uncertainty of  $\pm 0.005$ .

The most important theoretical error is, just as in the large  $x$  determinations [24], the uncertainty due to unknown higher order perturbative corrections. This is manifest both in the scheme dependence (results contrasting  $\overline{\text{MS}}$  and DIS schemes are presented in table 8), and the dependence on the choice of factorization scale  $M^2 \equiv k_1 Q^2$  and renormalization scale  $\mu^2 \equiv k_2 Q^2$  (table 8). Since at present there is insufficient data to rule out all but very large changes in these scales empirically,<sup>10</sup> we simply varied them by a factor of two either side, as is usual in the jet determinations [8]; this gives an uncertainty of  $+0.008 - 0.004$ . It could be argued that larger variations are already ruled out in deep inelastic scattering by the large  $x$  data [24].

The position of the quark thresholds is varied from  $\frac{1}{2}m_q$  to  $3m_q$  (with  $m_c = 1.5\text{GeV}$ ,  $m_b = 4.8\text{GeV}$ ), to give an overall uncertainty on  $\alpha_s(M_Z)$  of  $\pm 0.002$ : varying the prescription used for taking the running coupling across the thresholds gives a further uncertainty of  $\pm 0.001$ . To estimate the effect of higher twist corrections, and possible mass effects at the quark thresholds, we perform the analysis with a  $Q^2$  cut on the data, discarding all data with either  $Q^2 > Q_{\text{cut}}^2$ , or  $Q^2 < Q_{\text{cut}}^2$ . The results are displayed in table 9, and show a remarkable level of stability as  $Q_{\text{cut}}$  is varied. We can thus conclude that higher twist effects, since they would vary rapidly with  $Q^2$ , must be extremely small throughout the HERA region. Similarly any mass effects at the quark threshold must also have only a

---

<sup>10</sup> With the exception of significant reductions in the factorization scale.

small effect on  $\alpha_s$ : most of the statistical significance of our determination comes from the data points with the smallest values of  $x$ , and thus values of  $Q^2$  above the charm threshold but below the beauty threshold.

All these various possible sources of error are summarised in table 10: combining the theoretical errors in quadrature, we quote a value

$$\alpha_s(M_Z) = 0.120 \pm 0.005(\text{exp}) \pm 0.009(\text{th}). \quad (13)$$

This is quite consistent with other determinations, in particular those from fixed target deep inelastic scattering data [24], and the world average [8]. It is difficult to say at precisely which value of  $Q^2$  the result (13) is obtained, since the two loop running over quite a wide range of  $Q^2$  was a crucial ingredient in the match to the data [3], and thus to the determination of  $\alpha_s(Q^2)$ . However it should be clear from table 9 that the most important  $Q^2$  range is  $4\text{GeV}^2 \lesssim Q^2 \lesssim 100\text{GeV}^2$ .

To summarise, we have shown that perturbative QCD works extremely well in the kinematic region explored so far at HERA. This remains true even when the perturbation series is reorganised to sum all leading and next-to-leading large logarithms, though the data are as yet insufficient to show to what extent this is necessary. Furthermore, since the shape of  $F_2$  is then relatively free of nonperturbative uncertainties, varying rather rapidly with  $\alpha_s$ , it can be used to provide a surprisingly precise determination of  $\alpha_s$ . We have performed such a determination using the 1993 HERA data, with the result (13). The experimental error, while already relatively small, should improve substantially when the 1994 data become available, and the expected fivefold increase in statistics might also provide an empirical determination of the as yet unknown parameter  $x_0$ , and enable a reduction in the dominant theoretical error coming from the renormalization scale dependence. Although the present determination has much in common with jet determinations, it has the advantage that it is sufficiently inclusive that there are no uncertainties from hadronization, and in fact here higher twist effects seem to be very small indeed. Also, the summation of large logarithms is relatively easy to control, essentially due again to the inclusive nature of the measurement, but also to some accidental cancellations. This means that a further reduction in the theoretical error will presumably be possible with a calculation of the three loop anomalous dimensions for deep inelastic scattering, and of the subleading singularities at small  $x$ .

**Acknowledgements:** We would like to thank G. Altarelli, R.K. Ellis, R.G. Roberts, S. Catani, M. Ciafaloni, A. Cooper-Sarkar, F. Hautmann, R. Nisius and S. Bethke for various discussions during the course of this work.

## References

- [1] ZEUS Collaboration, *Zeit. Phys.* **C65** (1995) 379.
- [2] H1 Collaboration, *Nucl. Phys.* **B439** (1995) 471.
- [3] R. D. Ball and S. Forte, *Phys. Lett.* **B336** (1994) 77.
- [4] A. De Rujula, S.L. Glashow, H.D. Politzer, S.B. Treiman, F. Wilczek and A. Zee, *Phys. Rev.* **D10** (1974) 1649.
- [5] R. D. Ball and S. Forte, *Phys. Lett.* **B335** (1994) 77.
- [6] R.D. Ball and S. Forte, *Phys. Lett.* **B351** (1995) 313.
- [7] R.D. Ball and S. Forte, CERN-TH/95-132 [hep-ph/9505388](#) to be published in the proceedings of the XXXth Rencontres de Moriond, Les Arcs, March 1995.
- [8] G. Altarelli in ‘QCD - 20 Years Later’, Aachen, 1992;  
 S. Catani in ‘International Europhysics Conference on High Energy Physics’, Marseille, 1993;  
 S. Bethke in ‘QCD94’, Montpellier, 1994;  
 B.R. Webber in ‘XXVII International Conference on High Energy Physics’, Glasgow, 1994.
- [9] R.D. Ball and S. Forte, in the proceedings of “QCD94”, Montpellier, July 1994 (*Nucl. Phys. B (Proc. Suppl.)* **39B,C** (1995) 25).
- [10] S. Catani & F. Hautmann, *Phys. Lett.* **B315** (1993) 157, *Nucl. Phys.* **B427** (1994) 475;  
 F. Hautmann, to be published in the proceedings of “QCD94”, Montpellier, July 1994 (*Nucl. Phys. B (Proc. Suppl.)* ).
- [11] T. Jaroszewicz, *Phys. Lett.* **B116** (1982) 291.
- [12] S. Catani, F. Fiorani and G. Marchesini, *Phys. Lett.* **B234** (1990) 339;  
*Nucl. Phys.* **B336** (1990) 18;  
 S. Catani, F. Fiorani, G. Marchesini and G. Oriani, *Nucl. Phys.* **B361** (1991) 645.
- [13] S. Catani, M. Ciafaloni and F. Hautmann, *Phys. Lett.* **B242** (1990) 97;  
*Nucl. Phys.* **B366** (1991) 135; *Phys. Lett.* **B307** (1993) 147.
- [14] S. Catani & F. Hautmann, *Phys. Lett.* **B315** (1993) 157, *Nucl. Phys.* **B427** (1994) 475;  
 F. Hautmann, to be published in the proceedings of “QCD94”, Montpellier, July 1994 (*Nucl. Phys. B (Proc. Suppl.)* ).
- [15] S. Catani, DFF 207/6/94, talk given at *Les Rencontres de Physique de La Vallée d’Aoste*, La Thuile, 1994.
- [16] M. Ciafaloni, preprint CERN-TH/95-119 (May 1995).
- [17] S. Catani, unpublished (private communication).
- [18] R.K. Ellis, F. Hautmann and B.R. Webber, Cavendish-HEP-94/18, Fermilab-PUB-95/006-T, [hep-ph/9501307](#).

- [19] A.D. Martin R.G. Roberts and W.J. Stirling, *Phys. Lett.* **B306** (1993) 145.
- [20] W. Furmanski and R. Petronzio, *Zeit. Phys.* **C11** (1982) 437;  
M. Diemoz, F. Ferroni, E. Longo and G. Martinelli, *Zeit. Phys.* **C39** (1988) 21.
- [21] J.C. Collins and D.E. Soper, CTEQ-note-94-01, [hep-ph/9411214](#).
- [22] A.D. Martin, W.J. Stirling and R.G. Roberts, preprint RAL-95-021, DTP/95/14, [hep-ph/9502336](#).
- [23] M. Glück, E. Reya and A. Vogt, *Phys. Lett.* **B306** (1993) 391 and ref. therein.
- [24] A.D. Martin, W.J. Stirling and R.G. Roberts, *Phys. Lett.* **B266** (1991) 173;  
M. Virchaux and A. Milsztajn, *Phys. Lett.* **B274** (1992) 221.

## Figure Captions

Fig. 1. Double scaling plots of the 1993 HERA data on  $F_2^p$ : i)  $R_F F_2^p$  vs.  $\sigma$  for a) the ZEUS data [1], b) the H1 data [2]; ii) the same vs.  $\rho$ . The data plotted are those included in the fits but with the further cut  $Q^2 < 100\text{GeV}^2$ ;  $R_F$  is accordingly evaluated with  $n_f = 4$  and (as in [5])  $Q_0 = 1\text{GeV}$ ,  $x_0 = 0.1$  and  $\Lambda = 260\text{MeV}$ . The dotted, dashed, dotdash, and solid curves correspond respectively to double scaling, two loops, double leading  $Q_0\text{DIS}$ , and double leading DIS, with  $Q_0 = 2\text{GeV}$ ,  $x_0 = 0.1$ , and the remaining parameters fitted as in table 6. The curves in the  $\sigma$ -plots have  $\rho = 2.2$ : those in the  $\rho$ -plots  $\sigma = 1.7$ .

Fig. 2. Contours of equal  $\chi^2$  in the  $\lambda$ - $Q_0$  plane with  $\alpha_s(M_Z) = 0.120$ : a) at two loops,  $\overline{\text{MS}}$  scheme b) double leading DIS scheme with  $x_0 = 0.1$ .  $Q_0$  is in GeV. The  $\chi^2$  is computed in the same way as in table 4.

Fig. 3. As fig. 2, but the  $\alpha$  -  $\lambda$  plane, with  $Q_0 = 2$  GeV.

Fig. 4. As fig. 2, but now the  $Q_0$  -  $\alpha$  plane, with a)  $\lambda = -0.23$  in the two loop calculation and b)  $\lambda = -0.06$  in the double-leading calculation (see table 6).

$n$	$\tilde{a}_n[\overline{\text{MS}}]$	$c_n[Q_0\overline{\text{MS}}]$	$c_n[\overline{\text{MS}}]$	$\tilde{a}_n[Q_0\text{DIS}]$	$\tilde{a}_n[\text{DIS}]$
0	1	1	1	1	1
1	0.60112293	0.53664997	0.53664997	0.78145981	0.78145981
2	0.20235532	0.42906025	1.26303490	0.29913310	0.29913310
3	0.16029498	0.19506502	0.77061130	0.23767037	0.38806675
4	0.09325224	0.31745293	0.66181242	0.14877117	0.25256339
5	0.04811765	0.18492007	0.78619278	0.11628239	0.17838311
6	0.05656923	0.14537345	0.53159913	0.10092750	0.22632345
7	0.03508260	0.16442189	0.51841609	0.07337509	0.15473331
8	0.02509704	0.10681121	0.55225420	0.06616794	0.13891462
9	0.02919748	0.10018804	0.41447382	0.05783445	0.15744938
10	0.01903403	0.10015474	0.42612176	0.04649840	0.11602071
11	0.01660674	0.07307916	0.42532669	0.04371716	0.11532868
12	0.01780682	0.07253155	0.34787922	0.03845962	0.11997040
13	0.01250523	0.06820181	0.36161794	0.03308122	0.09568020
14	0.01206009	0.05472576	0.34791451	0.03142577	0.09846280
15	0.01202880	0.05482194	0.30399755	0.02796813	0.09707906
16	0.00917087	0.05018804	0.31366444	0.02513443	0.08291446
17	0.00919550	0.04317398	0.29683046	0.02389106	0.08559381
18	0.00874215	0.04291270	0.27186534	0.02157069	0.08203738
19	0.00717749	0.03903673	0.27677753	0.01992506	0.07384063

Table 1: Numerical values of the first twenty coefficients  $\tilde{a}_n$  and  $c_n$  in the  $Q_0$  schemes and  $\overline{\text{MS}}$  schemes. The  $\tilde{a}_n$  in  $Q_0\overline{\text{MS}}$  are the same as those in  $\overline{\text{MS}}$  by construction, while the  $\tilde{a}_n$  in DIS were given in ref.[6].

$n$	$\tilde{a}_n \times (4 \ln 2)^n$
0	1
1	$\frac{5}{3}$
2	$\frac{14}{9}$
3	$\frac{82}{81} + 2\zeta_3$
4	$\frac{122}{243} + \frac{25}{6}\zeta_3$
5	$\frac{146}{729} + \frac{14}{3}\zeta_3 + 2\zeta_5$
6	$\frac{2188}{32805} + \frac{287}{81}\zeta_3 + 12\zeta_3^2 + \frac{35}{9}\zeta_5$
7	$\frac{13124}{688905} + \frac{488}{243}\zeta_3 + \frac{515}{21}\zeta_3^2 + \frac{112}{27}\zeta_5 + 2\zeta_7$
8	$\frac{1406}{295245} + \frac{73}{81}\zeta_3 + \frac{55}{2}\zeta_3^2 + \frac{82}{27}\zeta_5 + 32\zeta_3\zeta_5 + \frac{15}{4}\zeta_7$
9	$\frac{11810}{11160261} + \frac{2188}{6561}\zeta_3 + \frac{2665}{126}\zeta_3^2 + 96\zeta_3^3 + \frac{1220}{729}\zeta_5 + \frac{1675}{27}\zeta_3\zeta_5 + \frac{35}{9}\zeta_7 + 2\zeta_9$
10	$\frac{177148}{837019575} + \frac{72182}{688905}\zeta_3 + \frac{20801}{1701}\zeta_3^2 + \frac{1342}{7}\zeta_3^3 + \frac{1606}{2187}\zeta_5 + \frac{5390}{81}\zeta_3\zeta_5 +$ $20\zeta_5^2 + \frac{451}{162}\zeta_7 + 40\zeta_3\zeta_7 + \frac{11}{3}\zeta_9$
11	$\frac{1062884}{27621645975} + \frac{2812}{98415}\zeta_3 + \frac{9563}{1701}\zeta_3^2 + \frac{9539}{45}\zeta_3^3 + \frac{8752}{32805}\zeta_5 + \frac{11972}{243}\zeta_3\zeta_5 +$ $440\zeta_3^2\zeta_5 + \frac{3710}{99}\zeta_5^2 + \frac{122}{81}\zeta_7 + \frac{1655}{22}\zeta_3\zeta_7 + \frac{56}{15}\zeta_9 + 2\zeta_{11}$
12	$\frac{1594324}{248594813775} + \frac{76765}{11160261}\zeta_3 + \frac{163553}{76545}\zeta_3^2 + \frac{1835119}{11340}\zeta_3^3 + 880\zeta_3^4 +$ $\frac{170612}{2066715}\zeta_5 + \frac{60268}{2187}\zeta_3\zeta_5 + \frac{159770}{189}\zeta_3^2\zeta_5 + \frac{34762}{891}\zeta_5^2 + \frac{949}{1458}\zeta_7 +$ $\frac{1729}{22}\zeta_3\zeta_7 + 48\zeta_5\zeta_7 + \frac{1066}{405}\zeta_9 + 48\zeta_3\zeta_9 + \frac{65}{18}\zeta_{11}$
13	$\frac{1913188}{1939039547445} + \frac{177148}{119574225}\zeta_3 + \frac{95149}{137781}\zeta_3^2 + \frac{113399}{1215}\zeta_3^3 + \frac{471136}{273}\zeta_3^4 +$ $\frac{19684}{885735}\zeta_5 + \frac{80738}{6561}\zeta_3\zeta_5 + \frac{73115}{81}\zeta_3^2\zeta_5 + \frac{75194}{2673}\zeta_5^2 + 624\zeta_3\zeta_5^2 +$ $\frac{7658}{32805}\zeta_7 + \frac{101311}{1782}\zeta_3\zeta_7 + 624\zeta_3^2\zeta_7 + \frac{20615}{234}\zeta_5\zeta_7 + \frac{1708}{1215}\zeta_9 +$ $\frac{3451}{39}\zeta_3\zeta_9 + \frac{98}{27}\zeta_{11} + 2\zeta_{13}$

Table 2: Exact expressions for the first fourteen coefficients  $\tilde{a}_n$  in  $\overline{\text{MS}}$  scheme.

$n$	$c_n \times (4 \ln 2)^n$
0	1
1	$\frac{43}{9} - \frac{\pi^2}{3}$
2	$\frac{1234}{81} - \frac{13\pi^2}{18} + \frac{4}{3}\zeta_3$
3	$\frac{7412}{243} - \frac{71\pi^2}{54} - \frac{2\pi^4}{15} + \frac{89}{9}\zeta_3$
4	$\frac{50012}{729} - \frac{233\pi^2}{81} - \frac{13\pi^4}{45} + \frac{910}{27}\zeta_3 - \frac{14\pi^2}{9}\zeta_3 + \frac{24}{5}\zeta_5$
5	$\frac{4129144}{32805} - \frac{1276\pi^2}{243} - \frac{71\pi^4}{135} - \frac{221\pi^6}{11340} + \frac{9074}{81}\zeta_3 - \frac{130\pi^2}{27}\zeta_3 + \frac{178}{9}\zeta_3^2 + \frac{808}{45}\zeta_5$
6	$\frac{190112792}{688905} - \frac{8384\pi^2}{729} - \frac{466\pi^4}{405} - \frac{2873\pi^6}{68040} + \frac{65864}{243}\zeta_3 - \frac{923\pi^2}{81}\zeta_3 - \frac{358\pi^4}{315}\zeta_3 + \frac{17939}{189}\zeta_3^2 + \frac{6536}{135}\zeta_5 - \frac{32\pi^2}{15}\zeta_5 + \frac{60}{7}\zeta_7$
7	$\frac{148801028}{295245} - \frac{45928\pi^2}{2187} - \frac{2552\pi^4}{1215} - \frac{15691\pi^6}{204120} - \frac{487\pi^8}{272160} + \frac{535846}{729}\zeta_3 - \frac{7456\pi^2}{243}\zeta_3 - \frac{2873\pi^4}{945}\zeta_3 + \frac{24988}{81}\zeta_3^2 - \frac{365\pi^2}{27}\zeta_3^2 + \frac{57896}{405}\zeta_5 - \frac{91\pi^2}{15}\zeta_5 + \frac{491}{5}\zeta_3\zeta_5 + \frac{1109}{42}\zeta_7$
8	$\frac{12320913596}{11160261} - \frac{301808\pi^2}{6561} - \frac{16768\pi^4}{3645} - \frac{51493\pi^6}{306180} - \frac{6331\pi^8}{1632960} + \frac{646232}{405}\zeta_3 - \frac{48488\pi^2}{729}\zeta_3 - \frac{18673\pi^4}{2835}\zeta_3 - \frac{4213\pi^6}{17010}\zeta_3 + \frac{1796639}{1701}\zeta_3^2 - \frac{7241\pi^2}{162}\zeta_3^2 + \frac{18620}{81}\zeta_3^3 + \frac{1189456}{3645}\zeta_5 - \frac{1846\pi^2}{135}\zeta_5 - \frac{926\pi^4}{675}\zeta_5 + \frac{98863}{270}\zeta_3\zeta_5 + \frac{1340}{21}\zeta_7 - \frac{58\pi^2}{21}\zeta_7 + \frac{112}{9}\zeta_9$
9	$\frac{1687431562504}{837019575} - \frac{1653376\pi^2}{19683} - \frac{91856\pi^4}{10935} - \frac{70499\pi^6}{229635} - \frac{34577\pi^8}{4898880} - \frac{2861\pi^{10}}{29937600} + \frac{398373436}{98415}\zeta_3 - \frac{368896\pi^2}{2187}\zeta_3 - \frac{28426\pi^4}{1701}\zeta_3 - \frac{15847\pi^6}{25515}\zeta_3 + \frac{13980418}{5103}\zeta_3^2 - \frac{55735\pi^2}{486}\zeta_3^2 - \frac{53756\pi^4}{4725}\zeta_3^2 + \frac{243592}{243}\zeta_3^3 + \frac{9349244}{10935}\zeta_5 - \frac{14446\pi^2}{405}\zeta_5 - \frac{7189\pi^4}{2025}\zeta_5 + \frac{833453}{810}\zeta_3\zeta_5 - \frac{4001\pi^2}{90}\zeta_3\zeta_5 + \frac{2234}{25}\zeta_5^2 + \frac{33265}{189}\zeta_7 - \frac{52\pi^2}{7}\zeta_7 + \frac{6612}{35}\zeta_3\zeta_7 + \frac{944}{27}\zeta_9$
10	$\frac{121977196479032}{27621645975} - \frac{10865024\pi^2}{59049} - \frac{603616\pi^4}{32805} - \frac{463216\pi^6}{688905} - \frac{113471\pi^8}{7348320} - \frac{37193\pi^{10}}{179625600} + \frac{2480052752}{295245}\zeta_3 - \frac{2296400\pi^2}{6561}\zeta_3 - \frac{885544\pi^4}{25515}\zeta_3 - \frac{393269\pi^6}{306180}\zeta_3 - \frac{100127\pi^8}{3207600}\zeta_3 + \frac{123059534}{15309}\zeta_3^2 - \frac{244417\pi^2}{729}\zeta_3^2 - \frac{468364\pi^4}{14175}\zeta_3^2 + \frac{11643262}{3645}\zeta_3^3 - \frac{33466\pi^2}{243}\zeta_3^3 + \frac{59513936}{32805}\zeta_5 - \frac{10208\pi^2}{135}\zeta_5 - \frac{45653\pi^4}{6075}\zeta_5 - \frac{43843\pi^6}{155925}\zeta_5 + \frac{780635}{243}\zeta_3\zeta_5 - \frac{1625\pi^2}{12}\zeta_3\zeta_5 + \frac{89374}{55}\zeta_3^2\zeta_5 + \frac{243391}{825}\zeta_5^2 + \frac{656708}{1701}\zeta_7 - \frac{3053\pi^2}{189}\zeta_7 - \frac{626\pi^4}{385}\zeta_7 + \frac{2125594}{3465}\zeta_3\zeta_7 + \frac{32156}{405}\zeta_9 - \frac{92\pi^2}{27}\zeta_9 + \frac{180}{11}\zeta_{11}$
11	$\frac{2004668634968152}{248594813775} - \frac{59521408\pi^2}{177147} - \frac{3306752\pi^4}{98415} - \frac{2537522\pi^6}{2066715} - \frac{155353\pi^8}{5511240} - \frac{203131\pi^{10}}{538876800} + \frac{242491\pi^{12}}{91945854000} + \frac{25554524638}{1240029}\zeta_3 - \frac{16901248\pi^2}{19683}\zeta_3 - \frac{6522752\pi^4}{76545}\zeta_3 - \frac{103219\pi^6}{32805}\zeta_3 - \frac{2539043\pi^8}{33679800}\zeta_3 + \frac{4336551098}{229635}\zeta_3^2 - \frac{1721324\pi^2}{2187}\zeta_3^2 - \frac{471014\pi^4}{6075}\zeta_3^2 - \frac{499339\pi^6}{170100}\zeta_3^2 + \frac{1697032087}{153090}\zeta_3^3 - \frac{340262\pi^2}{729}\zeta_3^3 + \frac{656023}{243}\zeta_3^4 + \frac{1336379576}{295245}\zeta_5 - \frac{687488\pi^2}{3645}\zeta_5 - \frac{341578\pi^4}{18225}\zeta_5 - \frac{185419\pi^6}{267300}\zeta_5 + \frac{85825556}{10935}\zeta_3\zeta_5 - \frac{531719\pi^2}{1620}\zeta_3\zeta_5 - \frac{464089\pi^4}{14175}\zeta_3\zeta_5 + \frac{8960074}{1485}\zeta_3^2\zeta_5 + \frac{17010553}{22275}\zeta_5^2 - \frac{819\pi^2}{25}\zeta_5^2 + \frac{5027845}{5103}\zeta_7 - \frac{23300\pi^2}{567}\zeta_7 - \frac{14209\pi^4}{3465}\zeta_7 + \frac{2334799}{1485}\zeta_3\zeta_7 - \frac{3034\pi^2}{45}\zeta_3\zeta_7 + \frac{6130}{21}\zeta_5\zeta_7 + \frac{254824}{1215}\zeta_9 - \frac{715\pi^2}{81}\zeta_9 + \frac{8414}{27}\zeta_3\zeta_9 + \frac{4313}{99}\zeta_{11}$

Table 3: Exact expressions for the first twelve coefficients  $c_n$  in  $\overline{\text{MS}}$  scheme.

	norm.		$\lambda$	$\chi^2$
a)	96%	104%	0	71.0
b)	96%	103%	$1.05 \pm 0.85$	64.8
	93%	100%	$-0.25 \pm 0.13$	59.7
	95%	101%	$-0.27 \pm 0.12$	58.6
c)	94%	100%	$-0.26 \pm 0.12$	59.5
	94%	100%	$-0.26 \pm 0.30$	59.6
d)	96%	102%	$0.08 \pm 0.12$	63.2
	97%	103%	$-0.13 \pm 0.17$	59.9
e)	98%	100%	$0.32 \pm 0.08$	132
	104%	107%	$-0.10 \pm 0.21$	137

Table 4: The fitted normalizations to the two experiments (H1 and ZEUS, with uncertainties of  $\pm 5\%$  and  $\pm 4\%$  respectively [21]), the fitted values of  $\lambda$  and the associated  $\chi^2$ s (for 121 degrees of freedom). All data points with  $\sigma, \rho > 1$  are included in the fits: this cut effectively excludes all points not inside the double scaling region. Statistical and systematic errors for each data point have been simply combined in quadrature. The different cases considered are a) the simple one loop double scaling calculation of ref. [5], with  $\lambda$  fixed ( $Q_0 = 1$  GeV); b) two loops ( $\overline{\text{MS}}$  scheme),  $Q_0 = 1$  GeV,  $Q_0 = 2$  GeV and  $Q_0 = 3$  GeV; c) two loops, DIS scheme, and double leading, SDIS scheme, both  $Q_0 = 2$  GeV; d) double leading  $Q_0 \overline{\text{MS}}$  scheme,  $Q_0 = 2$  GeV and  $Q_0 = 3$  GeV; e) as d), but  $\overline{\text{MS}}$  scheme. All entries b)-e) are full NLO computations with  $\alpha_s(M_Z) = 0.120$ ; the double leading calculations have  $x_0 = 0.1$ .

	norm.		$\lambda_q$	$\lambda_g$	$\chi^2$
a)	93%	100%	$-0.24 \pm 0.13$	$-0.33 \pm 0.48$	59.7
	96%	101%	$-0.12 \pm 0.02$	$-0.16 \pm 0.10$	59.8
	95%	101%	$0.01 \pm 0.04$	$-0.76 \pm 0.06$	68.8
b)	94%	101%	$-0.24 \pm 0.09$	$-0.52 \pm 0.23$	59.2
	97%	104%	$-0.12 \pm 0.02$	$-0.01 \pm 0.20$	62.5
	97%	103%	$0.10 \pm 0.06$	$0.01 \pm 0.37$	73.1
c)	96%	103%	$-0.23 \pm 0.05$	$0.10 \pm 0.07$	57.3
	96%	102%	$-0.25 \pm 0.02$	$0.03 \pm 0.16$	64.5
	96%	102%	$-0.26 \pm 0.02$	$0.12 \pm 0.17$	72.6
d)	95%	102%	$-0.23 \pm 0.05$	$0.14 \pm 0.10$	57.8
	95%	101%	$-0.25 \pm 0.02$	$0.02 \pm 0.05$	62.1
	96%	103%	$-0.26 \pm 0.02$	$-0.07 \pm 0.10$	68.1

Table 5: As table 4, but allowing  $\lambda_q \neq \lambda_g$ , and with various fitting and evolution procedures. The different cases considered are: a)  $\overline{\text{MS}}$  distributions evolved in  $\overline{\text{MS}}$ ; b)  $\overline{\text{MS}}$  distributions evolved in DIS; c) DIS distributions evolved in DIS; d) DIS distributions evolved in  $\overline{\text{MS}}$ . For each entry the three cases correspond respectively to two loops, double leading  $Q_0$  schemes, double leading, standard schemes. All calculations are done with  $\alpha_s(M_Z) = 0.120$ ; the two loop calculations have  $Q_0 = 2.0$ , and the double leading calculations  $Q_0 = 3$  GeV and  $x_0 = 0.1$ .

	norm.		$\lambda$	$\alpha_s(M_Z)$	$\chi^2$
a)	93%	100%	$0.42 \pm 0.56$	$0.1183 \pm 0.0092$	61.4
	95%	102%	$-0.23 \pm 0.03$	$0.1215 \pm 0.0017$	58.4
	96%	103%	$-0.26 \pm 0.02$	$0.1212 \pm 0.0017$	57.8
b)	94%	99%	$0.04 \pm 0.10$	$0.1186 \pm 0.0043$	64.2
	97%	103%	$-0.12 \pm 0.04$	$0.1200 \pm 0.0026$	59.9
c)	93%	100%	$-0.08 \pm 0.05$	$0.1144 \pm 0.0034$	62.5
	91%	98%	$-0.26 \pm 0.02$	$0.1106 \pm 0.0019$	65.7
d)	93%	99%	$-0.06 \pm 0.06$	$0.1140 \pm 0.0040$	64.9
	91%	98%	$-0.26 \pm 0.02$	$0.1098 \pm 0.0040$	67.8

Table 6: As table 4, but with  $\alpha_s(M_Z)$  now included in the fit: a) two loops, with  $Q_0 = 1$  GeV, 2 GeV, and 3 GeV respectively; b) double leading,  $Q_0 \overline{\text{MS}}$  scheme with  $Q_0 = 2$  GeV and 3 GeV; c) as b), but  $Q_0$  DIS scheme respectively; d) as b), but DIS scheme.

	norm.		$\lambda$	$\alpha_s(M_Z)$	$\chi^2$
a)	95%	102%	$-0.23 \pm 0.03$	$0.1215 \pm 0.0017$	58.4
b)	96%	102%	$-0.23 \pm 0.01$	$0.1224 \pm 0.0018$	57.8
c)	96%	103%	$-0.26 \pm 0.03$	$0.1224 \pm 0.0016$	58.1
	95%	101%	$-0.22 \pm 0.03$	$0.1211 \pm 0.0018$	59.1
d)	95%	102%	$-0.23 \pm 0.03$	$0.1212 \pm 0.0018$	58.7
	94%	101%	$-0.20 \pm 0.03$	$0.1202 \pm 0.0021$	59.7

Table 7: As table 5, but to demonstrate insensitivity to large  $x$  distributions and the fitting of the small  $x$  tail: all calculations at two loops with  $Q_0 = 2\text{GeV}$  and using a)  $D0'$ , b)  $D^-'$ , c)  $D0'$ , but now with  $\lambda_q = \lambda$ , and  $\lambda_g = \lambda + \Delta\lambda$ ,  $\Delta\lambda = -0.3, 0.3$ , d) using the two alternative fitting procedures described in the text.

	norm.		$\lambda$	$\alpha_s(M_Z)$	$\chi^2$
a)	95%	102%	$-0.23 \pm 0.03$	$0.1215 \pm 0.0017$	58.4
b)	96%	103%	$-0.25 \pm 0.03$	$0.1215 \pm 0.0017$	58.2
c)	94%	101%	$-0.42 \pm 0.03$	$0.1222 \pm 0.0014$	71.7
	96%	103%	$-0.13 \pm 0.04$	$0.1216 \pm 0.0022$	58.7
	98%	104%	$-0.08 \pm 0.05$	$0.1219 \pm 0.0024$	60.9
d)	95%	102%	$-0.14 \pm 0.05$	$0.1178 \pm 0.0024$	60.8
	95%	102%	$-0.20 \pm 0.04$	$0.1187 \pm 0.0024$	58.7
	95%	102%	$-0.25 \pm 0.03$	$0.1252 \pm 0.0018$	58.7
	95%	102%	$-0.27 \pm 0.03$	$0.1295 \pm 0.0024$	59.5

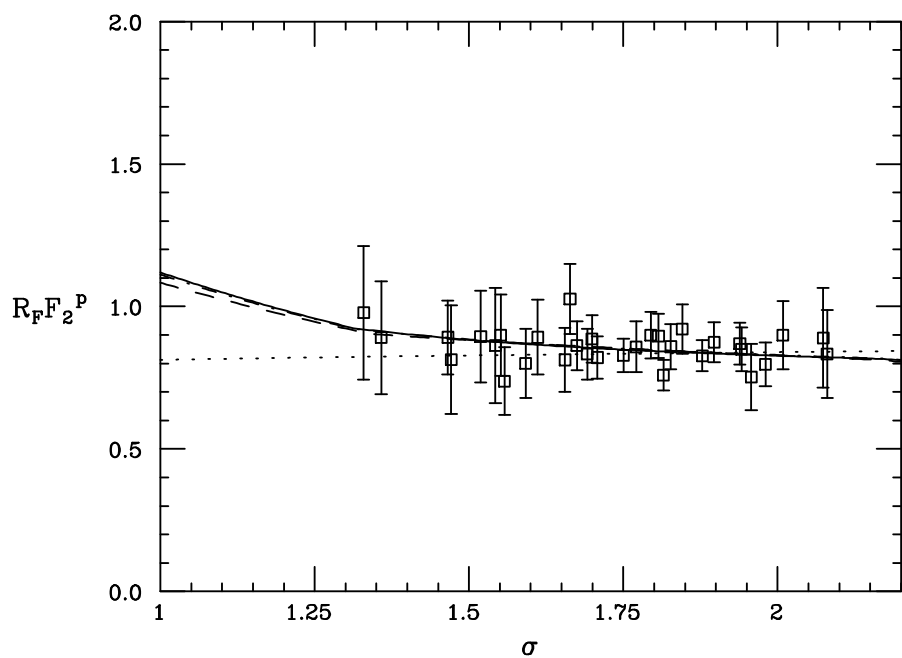
Table 8: As table 5, but to show the scheme dependence: all calculations at two loops with  $Q_0 = 2\text{GeV}$  and using a)  $\overline{\text{MS}}$  evolution, b) DIS evolution, c) as a), but with factorization scale  $k_1 = \frac{1}{2}, 2, 4$ , d) as a) but with renormalization scale  $k_2 = \frac{1}{4}, \frac{1}{2}, 2, 4$ .

$Q_{\text{cut}}$	norm.		$\lambda$	$\alpha_s(M_Z)$	$\chi^2$
10	95%	102%	$-0.24 \pm 0.04$	$0.1213 \pm 0.0015$	45/92
5	94%	102%	$-0.23 \pm 0.04$	$0.1211 \pm 0.0024$	22/53
4	96%	101%	$-0.22 \pm 0.06$	$0.1225 \pm 0.0031$	11/33
3.5	98%	100%	$-0.24 \pm 0.07$	$0.1220 \pm 0.0043$	6/20
3	101%	99%	$-0.33 \pm 0.13$	$0.1142 \pm 0.0177$	3/7
3	95%	103%	$-0.22 \pm 0.05$	$0.1219 \pm 0.0023$	54/111
4	96%	103%	$-0.21 \pm 0.10$	$0.1221 \pm 0.0034$	48/85
5	96%	103%	$-0.27 \pm 0.21$	$0.1216 \pm 0.0039$	44/77
7	99%	101%	$-0.39 \pm 0.35$	$0.1211 \pm 0.0064$	26/53

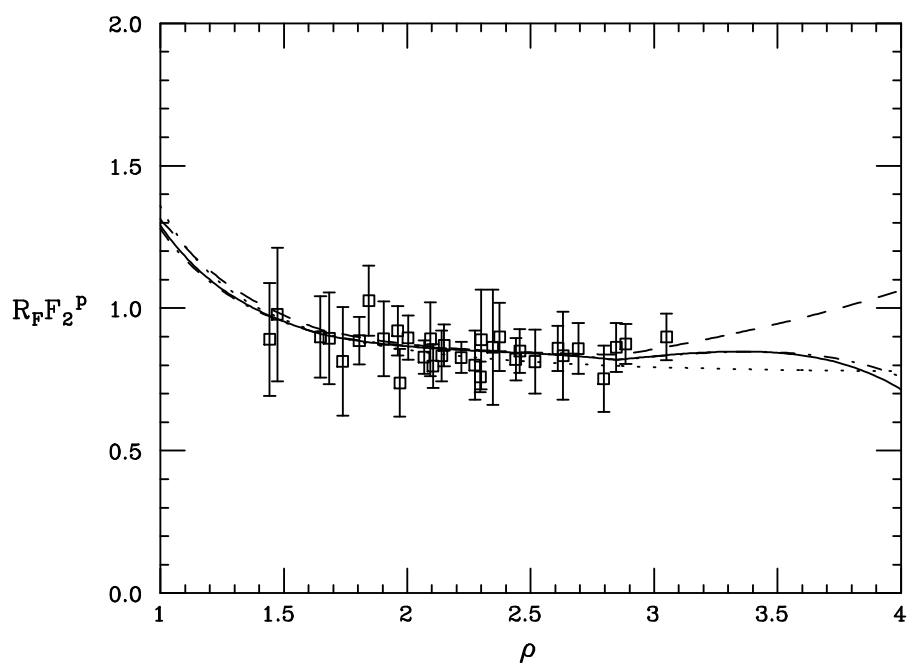
Table 9: As table 5, but to show the stability as the data are cut in  $Q$ : in the upper half of the table data above  $Q_{\text{cut}}$  are removed, while in the lower half data below  $Q_{\text{cut}}$  are removed.

two-parameter fit	$\pm 0.003$
variation of $Q_0$	$\pm 0.002$
fitting to large- $x$ p.d.f.	$\pm 0.003$
higher order singularities	$+0.002$ $-0.006$
position of thresholds	$\pm 0.002$
form of running coupling	$\pm 0.001$
higher twist corrections	$\pm 0.001$
scheme dependence	$+0.008$ $-0.004$

Table 10: Errors in the determination of  $\alpha_s(M_Z)$ .

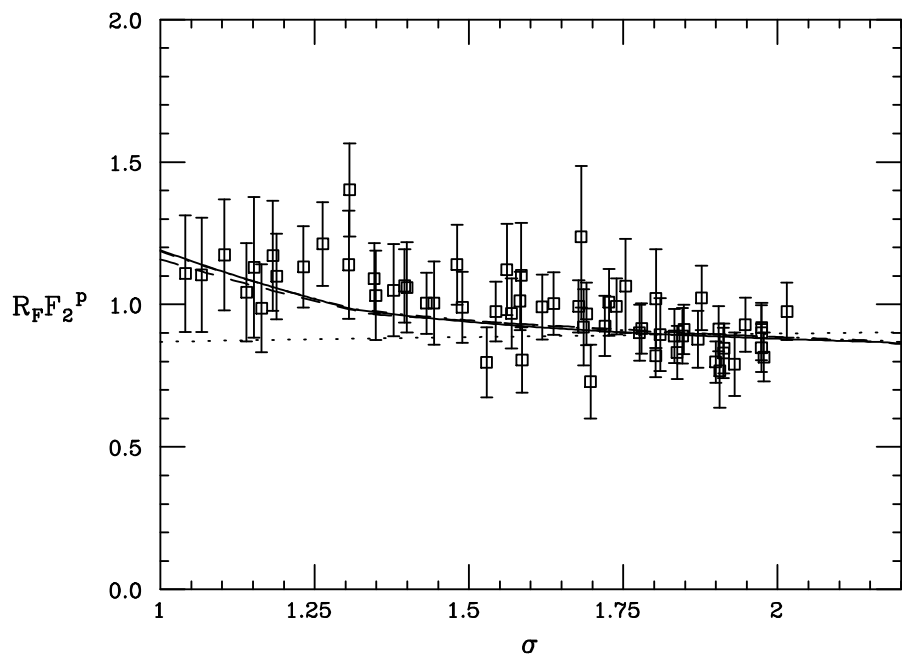


a (i)

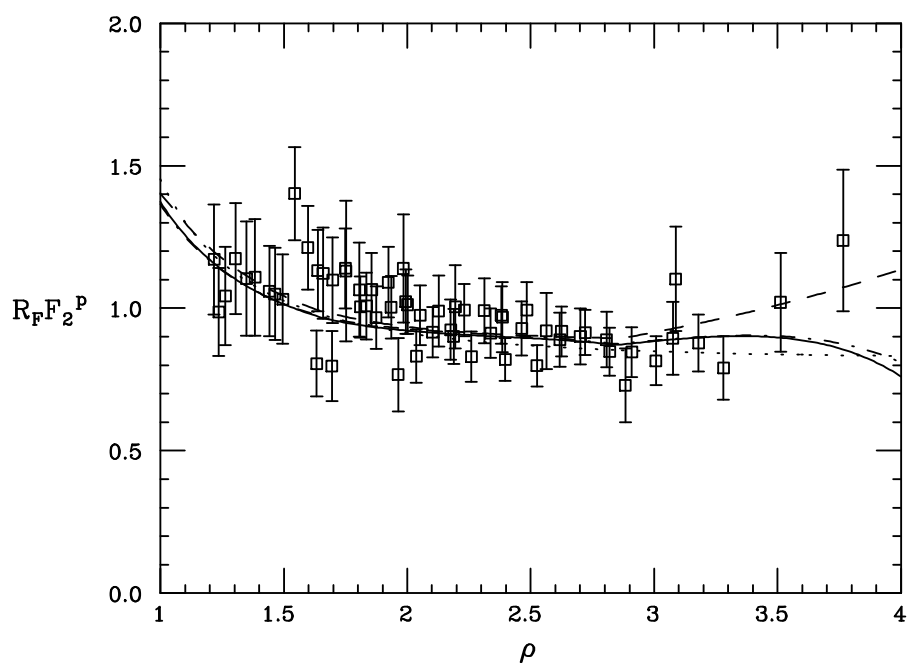


a (ii)

Fig. 1



b (i)



b (ii)

Fig. 1

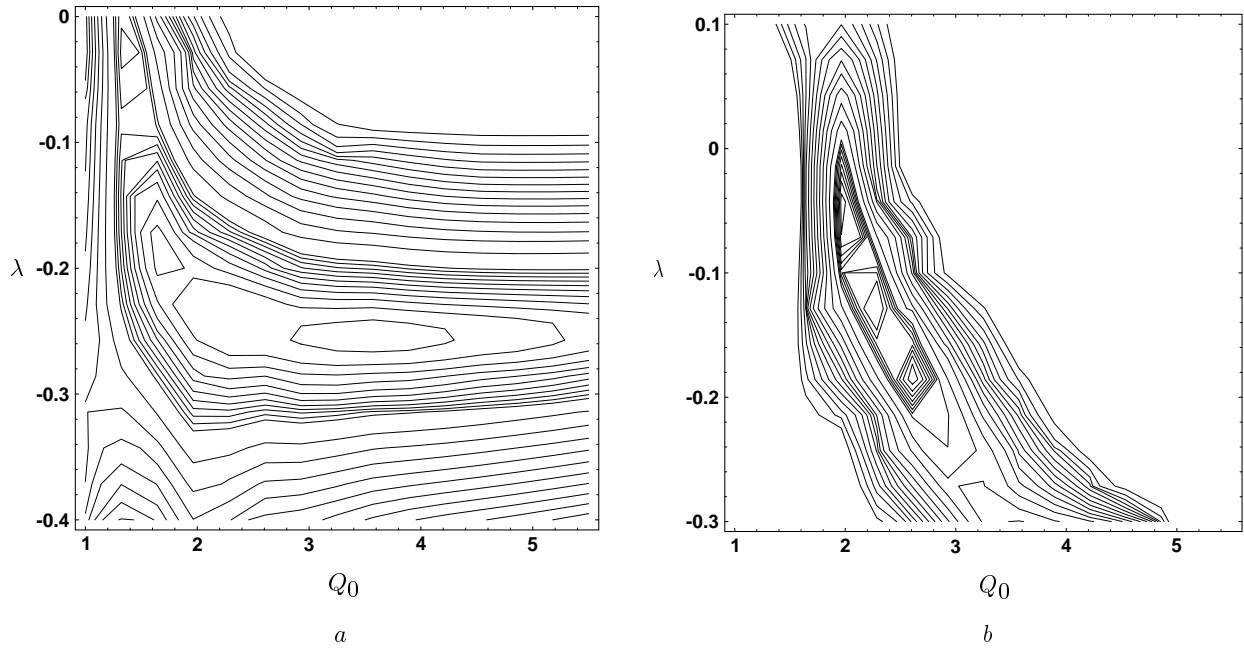


Fig. 2

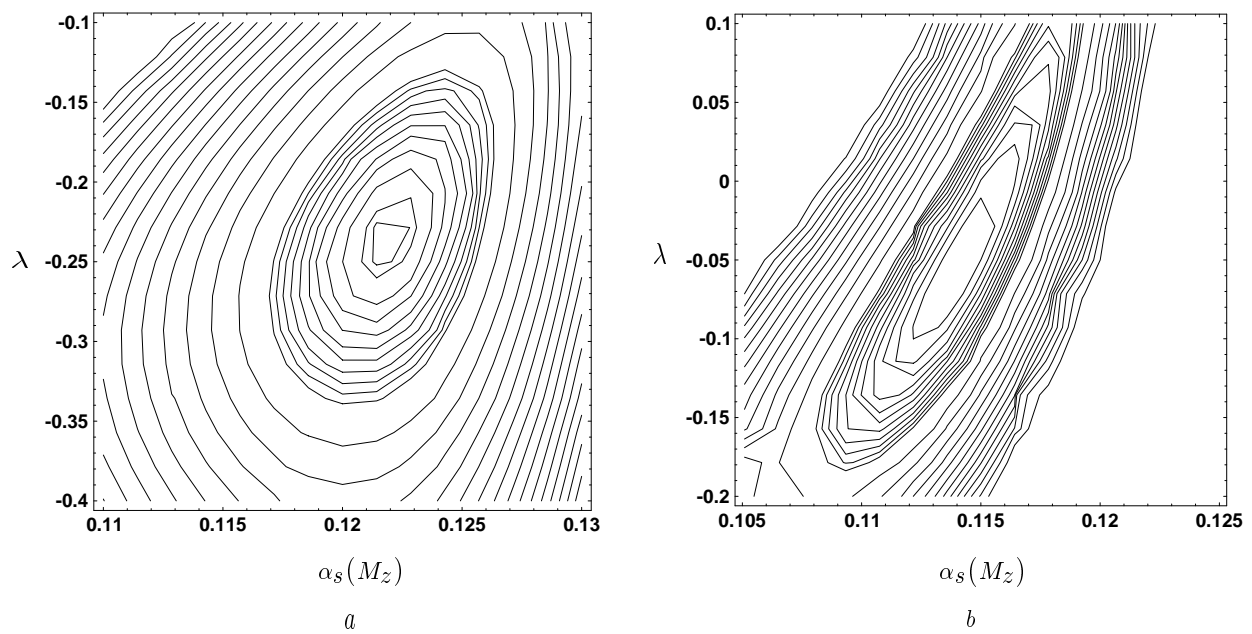
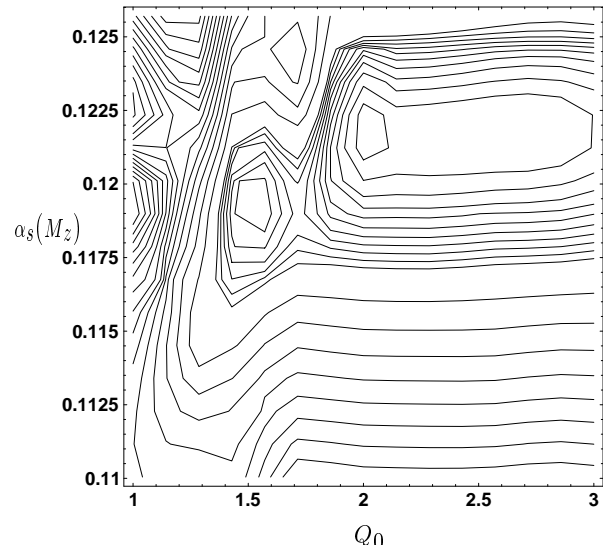
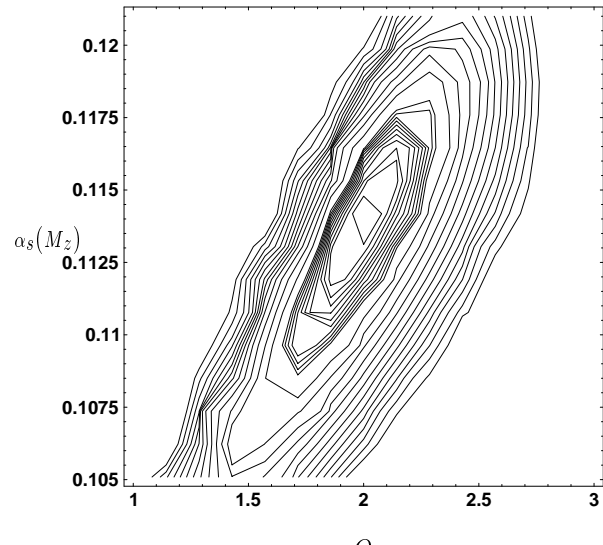


Fig. 3



*a*



*b*

Fig. 4